HoloGondel: in-situ cloud observations on a cable car in the Swiss Alps using a holographic imager

Alexander Beck, Jan Henneberger, Sarah Schöpfer, and Ulrike Lohmann

ETH Zurich, Institute for Atmospheric and Climate Science, Universitaetsstrasse 16, 8092 Zurich, Switzerland

Correspondence to: Jan Henneberger (jan.henneberger@env.ethz.ch)

Abstract. In-situ observations of cloud properties in complex alpine terrain where research aircraft cannot sample are commonly conducted at mountain-top research stations and limited to single-point measurements. The HoloGondel platform overcomes this limitation by using a cable car to obtain vertical profiles of the microphysical and meteorological cloud parameters. The main component of the HoloGondel platform is the HOLographic Imager for Microscopic Objects (HOLIMO 3G), which uses digital in-line holography to image cloud particles. Based on a two dimensional shadow-graph the phase resolved microphysical cloud parameters for the size range from small cloud particles to large precipitation particles are obtained. The low travelling velocity of a cable car on the order of $10\,\mathrm{m\,s^{-1}}$ allows measurements with high spatial resolution, however, at the same time it leads to an unstable air speed towards the HoloGondel platform. Holographic cloud imagers, which have a sample volume that is independent of the air speed are therefore well suited for measurements on a cable car. Example measurements of the vertical profiles observed in a liquid cloud and a mixed-phase cloud at the Eggishorn in the Swiss Alps in the winters 2015 and 2016 are presented. The HoloGondel platform reliably observes cloud droplets larger than $6.5\,\mu\mathrm{m}$, partitions between cloud droplets and ice crystals for a size larger than $25\,\mu\mathrm{m}$ and obtains a statistically significantly size distribution for every $5\,\mathrm{m}$ in vertical ascent.

1 Introduction

The role of clouds remains a large source of uncertainty in climate and weather models (Flato et al., 2013), ~~because our level of understanding of clouds is low.~~ In-situ measurements of the structure and the microphysical properties of clouds are important to gain a better knowledge of the radiative properties and the development of clouds (e.g., Sun and Shine, 1994; Morrison et al., 2012). Commonly these measurements are performed with a research aircraft (e.g., Verlinde et al., 2007; Vidaurre and Hallett, 2009; Heymsfield and Willis, 2014; Lawson et al., 2015), a helicopter (e.g., Siebert et al., 2006), a tethered balloon system (TBS) (e.g., Lawson et al., 2011; Sikand et al., 2013) or at mountain top research stations (e.g., Rogers and Vali, 1987; Uchiyama et al., 2014; Geerts et al., 2015; Vochezer et al., 2016). This paper introduces a novel approach for measuring in-situ properties of clouds on a cable car.

Airborne measurements have the ability to almost freely choose a flight path, which allows accurate control of time, in-cloud position and altitudes of the measurements. Multiple sampling of the same air mass in a Lagrangian manner is possible (Schumann et al., 2013), which allows to explore the evolution of specific atmospheric phenomena or events for up to several

hours. The possibility to equip an aircraft with a variety of in-situ instrumentation (aerosol, chemistry, cloud microphysics) gives the opportunity to collect a comprehensive data set of clouds. However, with true air speeds on the order of $100\,\mathrm{m\,s^{-1}}$ the spatial resolution of in-situ measurements on an airplane is limited, whereas in-situ measurements on a helicopter with a true air speed on the order of $20\,\mathrm{m\,s^{-1}}$ achieve much better results (Siebert et al., 2006). In addition, the high traveling speed of an aircraft causes ice shattering on the tips of the instruments (Baumgardner et al., 2012). Harsh conditions during flight operation (e.g. turbulence, lightning strikes, rapid change of temperature, pressure and relative humidity during decent and accent) and the need for an instrument safety certification make the instrument development a time-consuming and expensive process. In addition, the high operational costs of an aircraft make airborne campaigns expensive and a successful performance depends on a detailed planning up to several months or years in advance by larger groups of people to support the logistics it takes for an aircraft field campaign.

Tethered balloon systems can operate for an extended period of time (> 24 hours) and can measure the vertical profile of cloud properties from the surface to a height of $2\,\mathrm{km}$ and a wind speed below $10\,\mathrm{m\,s^{-1}}$ (Lawson et al., 2011). In comparison to airborne measurement, the main advantages are the higher spatial resolution, the reduced shattering of ice crystals and the lower operational costs. However, low payloads (< $15\,\mathrm{kg}$) and an operation only during low to moderate wind speeds (< $10\,\mathrm{m\,s^{-1}}$) limit their operational capability.

Ground-based measurements, like tethered balloon systems, can measure for as long as several hours or even days at low operational cost (Henneberger et al., 2013b). A spatial resolution comparable to a tethered balloon system can be achieved, because wind speeds are lower than the traveling speed of aircraft. However, ground-based measurements are limited to single-point observations of the cloud and are influenced by surface-based processes (Rogers and Vali, 1987; Geerts et al., 2015; Lloyd et al., 2015).

With the HoloGondel platform we introduce a novel approach to in-situ cloud measurements. The HoloGondel platform is designed to be mounted on a cable car to measure vertical profiles of cloud properties. Previous studies have already made use of cable cars to obtain vertical profiles of temperature and relative humidity (Reiter, 1967; Reiter and Carnuth, 1975; Gultepe and Zhou, 2011; Joe et al., 2012), aerosol measurements (Reiter and Carnuth, 1975) or ozone soundings (Reiter, 1967; Baumann et al., 2001; Piringer et al., 2001). The HoloGondel is equipped with instruments to observe the meteorological parameters of temperature, relative humidity and wind speed and direction. In addition, the HoloGondel platform uses digital in-line holography to image cloud particles and observe microphysical properties of clouds.

Digital in-line holography has been previously used in a series of airborne (Conway et al., 1982; Fugal and Shaw, 2009b; Beals et al., 2015) and ground-based field instruments (Conway et al., 1982; Raupach et al., 2006; Henneberger et al., 2013b). In comparison to other in-situ cloud probes, holographic imagers have specific advantages and disadvantages (see Baumgardner et al., 2011). Holography allows one to measure over a wide range of particle sizes. Because an image of the cloud particles is captured, no assumptions about the particle shape, orientation or refractive index is needed like in light scattering instrumentation. Holography also benefits from its well-defined sample volume, which is independent of particle size and air speed. This is of particular importance for the HoloGondel platform, because the air speed ~~towards~~ the instrument depends on the wind speed and the travel velocity of the cable car. Finally it provides the spatial distribution of the particles in the sample volume on a cm

scale (Beals et al., 2015). A disadvantage of holographic imaging systems is the high computational power required for data reconstruction and data analysis. However, with the progress in the development of an suitable software package (HOLOSuite Fugal, 2016) and the progress in computer technologies, data reconstruction and data analysis has become much faster.

Mounting the HoloGondel platform on a cable car enables ~~to obtain~~ vertical profiles in complex alpine terrain. This is a major step forward compared to single point measurements conducted at mountain top research stations. The portable design of the HoloGondel platform, unlike a tethered balloon system, enables easy shifts between different cable cars at different locations. ~~In addition, this approach offers the opportunity to obtain a vast set of vertical cloud profiles at only a fraction of the operational and organizational costs of a research aircraft.~~ The regular schedule of a cable car with up to 20 ascents and descents a day allows the observation of the temporal evolution of a single cloud. The combined observation of vertical profiles of the phase-resolved particle size distribution and the spatial distribution of cloud particles with the meteorological parameters can provide the necessary information to improve the level of understanding of clouds. For instance, ice crystal number concentrations (ICNCs) exceeding the number of ice nuclei by up to three orders of magnitude are observed at different mountain-top research stations (Henneberger et al., 2013b). These observations suggest that a surface-based ice multiplication process is active to produce the large ICNCs (Rogers and Vali, 1987; Geerts et al., 2015; Lloyd et al., 2015; Farrington et al., 2015). The HoloGondel platform is able to locate such high ICNCs dependent on the cloud height and at the height above the surface and can help to further investigate the origin of high ICNCs and possible multiplication mechanisms. Detailed information about the ice crystal habits from the pictures captured with the HoloGondel platform can be compared to ground-based (Shupe et al., 2008) and satellite (Zhang et al., 2010) remote sensing observations to improve their retrieval validation. Information about the ice crystal habit is also important to simulate the fall velocity of ice crystals (Baumgardner et al., 2011), which affects the lifetime of a cloud.

This paper describes the HoloGondel platform with its instrumentation (section 2), in particular the newly developed HOLographic Imager for Microscopic Objects (HOLIMO 3G) is introduced (section 3). In section 4, two case studies of microphysical measurements with the HoloGondel on the cable car from Fiescheralp to the Eggishorn in the canton Valais in Switzerland are discussed. Section 5 summarizes first experiences with the HoloGondel platform and offers suggestions for improvements of the HoloGondel platform and further research opportunities.

2 Description of the HoloGondel measurement platform

The HoloGondel platform is designed to perform in-situ cloud measurements on a cable car. Mounting a measurement platform on the roof of a cable car cabin requires the following design considerations:

First, the measurements platform must be light-weight, as an additional weight load due to a measurement platform reduces the admissible load weight of the cable car cabin. If this weight reduction leads to a reduced number of admissible passengers, the operators of the cable car might charge a fee for the installation of the measurement platform. Therefore, the measurement platform needs to be carefully designed with respect to its weight.

Second, low power consumption is important. Typically, the lack of an external power supply on a cable car cabin requires the platform to be operated with a battery. A battery capacity that allows a continuous operation of the platform at least during the operating hours of the cable car is suggested. A high battery drain of the platform would require a larger battery capacity and result in a higher weight. This is in contradiction to the first requirement and requires a careful selection of the power consuming components.

Finally, the different components of the measurement platform have to withstand the rough conditions on a cable car similar but not as severe to other in-situ cloud probes, e.g. as decribed in Spuler and Fugal (2011). These conditions include low temperatures (0 to $-20\,^{\circ}\mathrm{C}$), and moist, precipitating, and sometimes icing cloud environments and are potential dangers for the electronics of the instrument. In addition, ice falling ~~down on the instrument~~ from the ~~rope~~ or supporting masts of the cable car can strike the instrument.

The main component of the HoloGondel platform (Fig. 1) is the HOLIMO 3G instrument, which measures a phase-resolved size distribution, concentrations and water content (see section 3.1). The HOLIMO 3G instrument was designed to meet the requirements of the HoloGondel platform, i.e. low in power consumption and weight (see section 3.2). It consists of a single watertight box, which also houses the control and data-acquisition computer of the HoloGondel platform. The data is temporarily stored on two 1 TB solid-state drives (SSDs). Because of the large amount of data acquired ~~especially by the HOLIMO 3G instrument~~ (up to 1 TB per day) a local server storage (Synology NAS) is placed in the control room of the cable car. A wireless network adapter is installed to transfer the data from the instruments SSDs to the local server storage during the night. In addition, the HOLIMO 3G instrument is equipped with a mobile router, that ~~allows to~~ remotely access the instrument via the mobile data network.

The HoloGondel platform is also equipped with a 3D Sonic Anemometer (THIES), a heated temperature and humidity sensor (HygroMet4, Rotronic, $\pm$2-3 %RH for sub-zero temperatures, 4 Hz) built into a weather shed (RS24T, Rotronic) and a GPS Sensor (BU-353S4, GlobalSat). The entire setup is powered by two battery packs with a capacity of 1.5 kWh each, which is enough for continuous operation of the platform of at least 20 hours. The batteries can be fully recharged in 10 hours.

The wind measurements of the 3D Sonic Anemometer have to be corrected for the movement of the cable car relative to the actual wind velocity. For this correction the direction and the speed of the cable car relative to the surface was calculated from the GPS data and subtracted from the wind measurements. The relative humidity measurements on the HoloGondel platform are used only to indicate in-cloud conditions, because the measurement of the relative humidity in clouds is quite challenging. To protect the sensor from dew it is heated to a temperature of 8 K above the ambient temperature. Because of the accuracy of the humidity sensor of 2-3 %RH at sub-zero temperatures, we consider measurements above 95 %RH as in-cloud conditions.

The total weight of the HoloGondel platform is about 60 kg. The HOLIMO 3G instrument is the heaviest component with a weight of 18 kg followed by the two battery packs at 16 kg each. The additional meteorological instrumentation weighs 10 kg.

The HoloGondel platform is designed for modular operation and only the HOLIMO 3G as the main component is indispensable as it houses the control and data-acquisition computer for the entire platform. Additional instruments, e.g. aerosol instruments or other cloud probes, can independently be added to the setup only limited by the weight and power restrictions.

Also the battery packages can be used together or one at a time. Therefore, the HoloGondel platform can be adapted to the scientific question as well as the weight requirements of different cable cars.

3 HOLographic Imager for Microscopic Objects (HOLIMO 3G)

The HOLIMO 3G instrument is the third generation of holographic imagers developed over the last nine years (HOIMO I, Amsler et al. (2009); HOLIMO II, Henneberger et al. (2013b)) in the Atmospheric Physics group at the ETH Zurich and is designed for the use on a Gondola lift. HOLIMO 3G has an open path configuration allowing the ambient air to stream freely in-between the two towers and to observe the spatial distribution of the particle in the sample volume on a cm scale. In contrast, the predecessor HOLIMO II had an inlet aspirated with a calibrated flow powered by a pump. This meant compensating for non-isokinetic sampling and losing the spatial distribution of the particles in the sample. In addition, the open path configuration leads to a more compact design because heavy equipment like a pump to ensure a calibrated air flow is not necessary and helped to meet the weight requirements described in section 2.

3.1 Working Principle of HOLIMO 3G

The setup of a simple digital in-line holographic system is shown in Fig 2. The essential components are a laser as a coherent light source and a digital camera to record the image. In general, a lens is added behind the laser to collimate the light and a lens system is required in front of the digital camera to achieve the desired resolution (Spuler and Fugal, 2011). To acquire the single particle information with digital in-line holography, two steps are necessary (Fugal et al., 2009a). First, a particle, e.g. a liquid droplet or ice crystal, in the sample volume scatters the light and an interference pattern of the scattered wave and the reference wave is recorded. In a second step, single particle information is extracted from the recorded hologram using the open source HoloSuite software package (Fugal, 2016). In this step the hologram is reconstructed along the optical axis and the in-focus position of the particles is determined (Fugal et al., 2009a). The result is a set of two dimensional shadowgraphs, which are sorted into the three categories artifacts, liquid droplets and ice crystals using supervised machine learning based on a set of parameters (e.g. aspect ratio, minimal/maximal phase or amplitude value of a pixel, amplitude gradient in the shadowgraph, etc.) and the particle diameter is computed. To reduce the noise level in a hologram a background division is performed as described in (Fugal et al., 2009a). This method reduces the stationary noise, e.g. contamination on the optical components. To separate cloud droplets from ice crystals based on the shape of the particle a picture with at least a few pixels is needed. Following the considerations in Henneberger (2013a) the threshold to differentiate between cloud droplets and ice crystals was set to 25 µm, which corresponds to 8 times the pixel size. However, some ice crystals may be still misclassified as cloud droplets depending on their shape and orientation.

3.2 Instrument Description

Due to the open path configuration of the newly designed HOLIMO 3G instrument, it was possible to reduce the weight by more than a factor of two compared to its predecessor HOLIMO 2. This was possible, because several components (e.g. blower,

flow-meter, heating, rotor) of the HOLIMO 2 setup, necessary for the inlet based design, are not required for the HOLIMO 3G instrument. In addition, the components of the new instrument were carefully selected with respect to their weight (e.g. single-board computer, polycarbonate housing).

The new design of the HOLIMO 3G instrument is distinguished by its two towers on top of the hermetically-sealed box (Fig. 3), which houses a single board computer (ADLE3800PC, ADL Europe, Germnay), two 1 TB SSDs (Samsung 840 EVO), a mobile router (RBMTXI, M2M, Germany) and a laser. The single board computer is installed because of its compact design and low power consumption. Solid-state drives are used because of their ruggedness in regard to possible vibrations on top of the cable car. The passively Q-switched Nd:YAG laser with a wavelength of 532 nm (FDSS532Q4, CryLas, Germany) emits pulses with a width of 1.4 ns and a pulse energy of 42 µJ. Behind the laser head the laser beam is attenuated using a notch filter and coupled into a fiber to transport the beam to one of the towers. The fiber also cleans the laser profile, because only the lowest transverse electromagnetic mode is transmitted. Behind the fiber, the laser beam is collimated to a diameter of 40 mm with a lens mounted in the tower. Windows are installed in the white tips of the two towers to allow the laser beam to exit and re-enter the instrument. The windows are made of sapphire because of its high heat conductivity ($\approx 23\,\mathrm{W\,mK^{-1}}$) compared to the standard N-BK7 glass and are heated to prevent freezing and evaporate cloud particles stuck to the window. The distance between the sapphire windows is 24 cm.

At the bottom of the second tower a 30 MP camera (HR29050, SVS-Vistek, Germany) with a pixel size of 5.5 µm is installed to capture the hologram. On top of the camera a bi-telecentric lens system (Sill Optics S5LPJ3618/M58) with a magnification of 1.8 and a numerical aperture of 0.11 is mounted. The described setup achieves a resolution of 6.2 µm within a distance of approx. 75 mm from the sapphire window of the tower with the camera and lens-system (see Sect. 3.3). With a cross sectional area of 20 mm x 13.4 mm the corresponding sample volume is 17 $\mathrm{cm^3}$. The entire sample volume between the towers is 60 $\mathrm{cm^3}$ and has a reduced resolution of 20 µm. Whereas the smaller sample volume with a high resolution enables to observe both the smaller liquid droplets and larger ice crystals, the large sample volume can be used to obtain better statistics of the few ice crystals. With a maximal frame rate of 6 fps this results in a sample volume rate of 100 $\mathrm{cm^3 s^{-1}}$ for the small sample volume and 360 $\mathrm{cm^3 s^{-1}}$ for the entire detection volume in-between the two tours. Data presented in this work is only extracted from the small sample volume. ~~However, the entire detection volume in-between the two tours can be used to get a better statistics for the larger but fewer ice crystals.~~

For the smaller sample volume of 17 $\mathrm{cm^3}$ and a droplet concentration on the order of 100 $\mathrm{cm^3}$, the Poisson counting error is less than 3 %. However, for the much fewer ice crystals on the order of 100 $\mathrm{L^{-1}}$ the Poisson counting error yields ~~25~~ % for a single hologram and the small sample volume. Because only the small sample volume is used for the analysis of the ice crystals for the data presented in this work, at least 10 holograms are grouped together to decrease the Poisson counting error for the ice crystals to a value below 8 %, respectively below 1 % for the cloud droplets.

3.3 Resolution Measurements

As described in Henneberger et al. (2013b) the resolution of a holographic system is limited by three constraints. One limitation is imposed by the pixel size of the camera (D_{pixel}) and the magnification of the lens system (M)

$$D_{\text{res,pixel}} = \frac{2D_{\text{pixel}}}{M}. \tag{1}$$

The remaining two resolution limiting aspects can be calculated using the Rayleigh criterion

$$D_{\text{res}} = \frac{1.22\lambda}{NA} \tag{2}$$

with the wavelength λ and the numerical aperture NA, which is a representation of the acceptance angle of the optical system. The numerical aperture of the lens system (NA_{lens}) is a property of the lens design resulting in a resolution limit

$$D_{\text{res,lens}} = \frac{1.22\lambda}{NA_{\text{lens}}} \quad . \tag{3}$$

The numerical aperture of the optical setup of a holographic system can be calculated from its effective aperture D_{eff} and the reconstruction distance z_{rec}

$$NA_{\text{lens}} \approx \frac{D_{\text{eff}}}{2z_{\text{rec}}} \quad . \tag{4}$$

The resulting resolution limit $D_{\text{res,rec}}$ is therefore a linear function of the reconstruction distance z :

$$D_{\text{res,rec}} = \frac{2.44\lambda}{D_{\text{eff}}} \times z_{\text{rec}} \quad . \tag{5}$$

The strongest constraint of the above mentioned resolution limits restricts the optical resolution of the instrument. To ensure a high resolution over a large reconstruction distance, the optical parameters of the components have to be carefully matched. For reconstruction distances $z < 8\,\text{cm}$, the pixel size limits the resolution of the HOLIMO 3G instrument with a theoretical resolution limit of $D_{\text{res,pix}} = 6.2\,\mu\text{m}$. For larger reconstruction distances $D_{\text{res,rec}}$ dominates (Fig. 4).

The theoretical considerations of the resolution limits of the instrument were verified with laboratory measurement using ~~an~~ US Air Force high resolution target (1951 USAF) as it was done by Spuler and Fugal (2011). The target is a glass plate with a series ~~of a~~ pattern of three horizontal and three vertical bars where the distance between the bars is twice their width. The optical resolution limit of the evaluated system is defined by the distance between the bars of the smallest pattern of which both the three horizontal and vertical lines can still be resolved. During the measurements the target was placed at various position inside of the sample volume. Within a reconstruction distance of $1\,\text{cm} < z < 8\,\text{cm}$ the measurements are close to the theoretical resolution limit of $6.2\,\mu\text{m}$ (Fig. 4). Also the observed increase of the resolution limit due to $D_{\text{res,rec}}$ for reconstruction distance larger than $8\,\text{cm}$ is in good agreement with the theoretical considerations. Only for reconstruction distances $z < 1\,\text{cm}$ the observations deviate from the theoretical calculations. Likely the twin image, which is more pronounced at small z distance and bigger particle size disturbs the finding of the focus plane, and impairs the sizing of the object.

3.4 Calibration of HOLIMO 3G

The sizing algorithm of the HOLOSuite software package was calibrated for the HOLIMO 3G instrument following Henneberger et al. (2013b). Cross-linked poly methyl methacrylate (PMMA) spheres (colloquial acrylic glass) of diameters 6.4, 10.25 and 18.23 µm and a density of $\rho = 1180\,\mathrm{kg\,m^{-3}}$ were suspended in the air using a Fluidized Bed Aerosol Generator (TSI, Minnesota USA). Their size was measured with the HOLIMO 3G instrument and an Aerodynamic Particle Sizer (APS, TSI, Minnesota USA). The results for HOLIMO 3G are normalized to the maxima of the respective size distribution and a Gaussian distribution is fitted for the three sample sizes (Fig. 5). These results and the results of the APS are compared to the nominal diameter measured by the manufacturer (Microbeads, Norway) with a COULTER Multisizer 3 (Table 2).

Both, the results of the APS and the HOLIMO 3G instrument agree with the nominal diameter within their uncertainties. Although a trend towards an overestimation of the spheres with a smaller diameter is visible, a size correction similar to the one introduced by Henneberger et al. (2013b) is not applied, because all the results agree within in the square root of a pixel size with the nominal diameter. This is in agreement with a study by Lu et al. (2008), which shows a similar accuracy of the algorithm for larger particle sizes.

4 Field measurements

4.1 Description of the measurement site

The field measurements were conducted on the cable car between the Fiescheralp (46°24′N 8°06′E) and the Eggishorn (46°25′N 8°05′E) in the canton Valais in Switzerland (see Fig. 6, right). Over a horizontal distance of 1716 m it covers a vertical elevation of 654 m, with a maximum altitude of 2871 m.a.s.l.. During a ride of the cable car its height above the surface varies between 20 and 110 m (see Fig. 6, left). An overview on the technical parameters of the cable car is given in Table 3.

The setup of the HoloGondel platform during the campaign in winter 2016 is shown in Fig. 1. The instruments (HOLIMO 3G, Sonic, Temp/RH) are mounted on the downhill facing side of the cable car approx. 1.20 m above the roof of the cable car cabin. In winter 2015, the instrumentation was the same except temperature, humidity and wind sensors were not present, just the HOLIMO 3G and the GPS.

We present two case studies one each from the campaigns in winter 2015 and 2016. The first case study represents a situation with a liquid cloud (hereafter referred to as "Liquid Case") that was observed on 23 February 2016. The second case study represents a situation with a mixed-phase cloud (hereafter referred to as "Mixed-Phase Case") on 21 March 2015.

During the Liquid Case, the temperature at the Eggishorn varied between - 8 ° and - 5 °C. On this day a cold front was moving from the north towards the Alps resulting in a predominant wind direction at the Eggishorn from the west with wind speeds between 2 and 8 $\mathrm{m\,s^{-1}}$. A patchy cloud cover in the morning and a uniform cloud cover in the afternoon was observed from satellite pictures, but no precipitation was detected by the radar. During the Mixed-Phase Case, the temperature varied between - 7 ° and - 4 °C and a low pressure system over north-east Germany led to a south-westerly flow with wind speeds up

to 5 $\mathrm{m\,s^{-1}}$ at the Eggishorn. ~~At~~ this day a cirrus cloud layer was observed from satellite pictures above the Eggishorn, but also no precipitation.

During one ascent or descent with the cable car, the HoloGondel platform captures a maximum of 1200 holograms. For the Liquid Case an average of 240 holograms are analyzed for each run of the cable car. With a total of 10 runs this corresponds to a sampled air volume of approximately 40 L. For one run of the Liquid Case the maximal number of 1200 holograms, respectively 20 L of air is analyzed. For the Mixed-Phase Case 120 holograms are reconstructed per run, which corresponds to a total sampled air volume of about 8 L for a total of 4 runs. At least 10 holograms are grouped together to a sample volume of 0.17 L to obtain a better counting statistics when vertical profiles are presented. This results in a maximal vertical resolution of 5 m (Fig.9). For a uniform presentation of the data of the Liquid and Mixed-Phase case the data is presented in 75 m intervals, which corresponds to 40 holograms for the Liquid Case and 20 holograms for the Mixed-Phase Case. An exception is the presentation of the height-resolved size distribution for the Liquid Case in Fig. 8. For a clearer presentation this data is averaged over 4 height intervals of 150 m.

4.2 Liquid Case

For the analysis the data of 23 February 2016 is split into two groups representing different cloud behaviors.

During the morning the height profiles of the meteorological parameters (Fig. 7) imply relatively steady conditions with a constant wind from West-Southwest independent of the altitude. The median wind speed ~~of~~ the vertical intervals decreased from 6 $\mathrm{m\,s^{-1}}$ at the Fiescheralp to 2 $\mathrm{m\,s^{-1}}$ at the Eggishorn. The reported relative humidity persistently exceeded 96 % independent of the altitude and time. Considering the accuracy of the relative humidity sensor this has to be assumed as in-cloud conditions. The median temperature ~~of~~ the vertical intervals ranged between -6.2 and -3.5 $^{\circ}$C.

The cloud droplet number concentration (CDNC) varied with altitude and over time (Fig. 7) in the morning of 23 February 2016. During the first run in the morning almost no cloud droplets were observed with the HOLIMO 3G instrument (< 5 $\mathrm{cm^{-3}}$). Later in the morning a CDNC up to 280 $\mathrm{cm^{-3}}$ was present at altitudes below 2500 m. Smaller CDNC of 100 $\mathrm{cm^{-3}}$ or less were observed close to the Eggishorn. The height resolved size distribution of the run at 8:51 (Fig. 8) shows a decrease of mean droplet diameter from 11.8 to 10.6 µm with decreasing altitude.

The observations can be explained by fog that was formed lower in the valley, rose in the early morning and continued to persist with its cloud top at an altitude of 2500 m. This temporal evolution was also observed by the webcam pictures of the Eggishorn and the Fiescheralp. After 9:41 the cloud top began to sink again. This can be explained by the evaporation of the cloud droplets at the cloud top due to absorption of solar radiation. The observed CDNC of 150 to 250 $\mathrm{cm^{-3}}$ and a droplet size of 11 µm is in the range for fog or stratus clouds (Lohmann et al., 2016).

During the early afternoon the observed meteorological conditions were similarly stable as in the morning (Fig. 7). The temperature was nearly the same, wind speed was a little higher (up to 10 $\mathrm{m\,s^{-1}}$) and the wind direction near the top station turned towards south. Only the relative humidity showed a higher variability with values as low as 94 % at an altitude of 2500 m. This observation is reflected by the measurements of the CDNC, which vary highly over time at an altitude of 2600 m.

At 12:51, 13:11 and 13:51 CDNCs between 280 and 420 cm^{-3} are observed. The concentration is close to 0 cm^{-3} for the runs at 13:31 and 14:12. This indicates a pocket of clear air at an altitude of 2600 m (see also Fig. 9).

The CDNC was typically around 200 cm^{-3} during the afternoon. Remarkable is the observation of a CDNC as high as 400 cm^{-3} at an altitude of 2500 m at 13:51, which is still within the range of typical values for stratus clouds (Lohmann et al., 2016). Although the background in a hologram increases at such high number concentrations manual inspection of the classified particles has shown that the algorithm is still capable to reliably distinguish between artifacts and cloud droplets.

Although a uniform cloud cover was observed from satellite pictures above the Eggishorn in the afternoon, the observation shows a high variability of the CDNC at an altitude of 2600 m. In-between two runs of the cable car the CDNC alternates between 350 cm^{-3} and less than 50 cm^{-3}. This illustrates the capability of the HoloGondel platform to observe the temporal evolution of a cloud with a resolution of twenty minutes. With a mean horizontal wind speed of 5 $\mathrm{m\,s}^{-1}$ this corresponds to a variation in the vertical cloud structure over a horizontal distance of 6 km or less. The height resolved size distribution in Fig. 8 shows an increase of the mean cloud droplet diameter from 10 to 15 $\mu\mathrm{m}$ with increasing altitude. This is expected in a cloud dominated by condensational growth (Lohmann et al., 2016) and in agreement with lidar observations of shallow tropical cumuli, which show a sharp increase of the effective radius above cloud base (McFarlane and Grabowski, 2007).

In Fig. 9 the vertical profiles of the CDNC and mean diameter with the maximal vertical resolution of the HoloGondel platform of 5 m is shown and compared to the vertical profiles with a resolution of 75 m for the run at 13:31 on 23 February 2016. At least 10 holograms are grouped together resulting in a Poisson counting error of less than 3 $\%$. From the vertical profile of the CDNC the extend of the pocket of dry air is clearly visible. Below an altitude of 2700 m the CDNC decreases within a vertical interval of less than 100 m from more than 200 cm^{-3} to less than 10 cm^{-3}. It remains at such low values for 50 m before it increases within an interval of 50 m back to a value larger than 200 cm^{-3} below an altitude of 2500 m. In the same altitude interval the decrease in the mean cloud droplet diameter due to the evaporation in the pocket of dry air is visible from the high-resolution vertical profile. Besides the pocket of dry air at an altitude of 2600 m, variations of the CDNC of more than 100 cm^{-3} are observed in the altitude intervals 2800 - 2700 m and 2400 - 2300 m and illustrates the capability of the HoloGondel platform to observe the variability of the cloud structure on the order of several meters.

4.3 Mixed-Phase Case

During the first campaign at the Eggishorn in the winter 2015 only the HOLIMO 3G instrument was mounted on the HoloGondel platform. Therefore the analysis of the Mixed-Phase Case on 21 March 2015 is limited to the height profiles of the microphysical parameters and the meteorological observation of the MeteoSwiss station at the Eggishorn.

The noise level of the holograms captured during the campaign in 2015 was considerably higher due to mechanical instabilities of the optical setup of the HOLIMO 3G instrument. As a consequence the separation between cloud droplets and ice crystals was possible only for particles larger than 35 $\mu\mathrm{m}$. Therefore, all particles smaller than 35 $\mu\mathrm{m}$ are classified as cloud droplets. As the ice crystal number concentration is two to three orders of magnitude smaller than for the CDNC this has only little effect on the results for the CDNC and mean diameter.

Fig. 10 shows the height profiles for the number concentration, mean diameter and water content of the cloud droplets and ice crystals. The height profiles of the CDNC show a similar trend during this morning: The number concentration decreases with decreasing altitude to a value of less than $20\,\mathrm{cm}^{-3}$ below 2300 m before 11:00 and below 2400 m after 11:00. Also the profiles of the mean cloud droplet diameter do not show a high temporal variability during the presented time interval. The profiles show a maxima of the mean diameter at an altitude of 2600 m. Above this altitude the mean diameter decrease to a value of 16 µm and below this altitude it decreases to a value of 13 µm at 2300 m. The decrease of the CDNC at altitudes below 2500 m suggests either a completely glaciated cloud or an cloud base near the Fiescheralp. Both possibilities explain the rapid decrease of the mean cloud droplet diameter due to the evaporation in sub-saturated air with respect to liquid water.

The height profiles of the ICNC show a much higher temporal and vertical variability. The ICNC ranges from 20 to more than $150\,\mathrm{L}^{-1}$ in-between the different runs and varies by more than a factor of three in the profile at 09:31. However, below 2400 m the ICNC consistently drops below $50\,\mathrm{L}^{-1}$. The profiles of the mean ice crystal diameter and the ice water content (IWC) increase with decreasing altitude over the entire altitude interval for the runs at 09:31, and 09:53. A rapid growth of the ice crystals at the expense of the cloud droplets is expected in a mixed-phase cloud due to the Wegener-Bergeron-Findeisen process (Wegener, 1911; Bergeron, 1935; Findeisen, 1938). The profile of the runs at 11:13 and 11:31 show a minimum in mean ice crystal diameter at an altitude of 2600 m and the IWC is decreasing with decreasing altitude. The vertical profiles have in common that the ratio of the ice water content to the total water content (IWC/TWC) is increasing with decreasing altitude. For the run at 11:13 the ratio IWC/TWC is close to one indicating a completely glaciated cloud. However, webcam pictures from the Fiescheralp suggest that the cloud base was above the lower cable car station and a few ice crystals fell out and were observed with the HoloGondel instrument.

An interesting feature is the high variability of the ICNC especially during the run at 09:31 (Fig. 10). Possible mechanism for the high variability of ICNC can only discussed briefly, because the meteorological parameters were not measured with the HoloGondel platform in 2015. Very localized high ice nucleation rates cannot explain the observed variability of the ICNC at the observed temperature of -5 °C. An influence due to ground-based processes are not expected because the cable car is more than 50 m above the surface at an altitude of 2600 m where the highest ICNC were observed and a much lower ICNC was observed where the cable car was closer to the surface. Another possibility is a varying concentration of ice crystals that fall into the cloud from a higher lying ice cloud above the Eggishorn as it was observed on satellite pictures. Finally the Hallet-Mossop process is a possible mechanism to explain the very localized spikes of high ICNC, which is active at this temperature and can significantly increase the ICNC (Hallet and Mossop, 1974).

It is important to mention that the cable car is above the ski slope during its ride and the production of artificial snow with snow canons can be a possible explanation for the high variability in the ICNC. Only small variations in the wind speed and direction due to local turbulence can lift the artificial snow to very different locations and may explain the high variability of the ICNC. Further investigation of the ice crystal habit from their two dimensional shadowgraph is also available with the HOLIMO 3G instrument and can help to solve this problem, but was not realized for this case study.

A unique feature of holography is the information about the spatial distribution of the cloud particles within the sample volume captured in a single hologram (Fig. 11). The presented examples are from the run at 9:31. The spatial distribution on

top of Fig. 11 represents a cloud at an altitude of 2600 m with a ICNC larger than 100 L^{-1} and a CDNC larger than 100 cm^{-3}. Whereas the cloud droplets are distributed uniformly within the sample volume the ice crystals are concentrated within 30 mm. This reflects the high variability of the ICNC compared to the CDNC discussed above. The spatial distribution on the bottom of Fig. 11 was taken at an altitude of 2300 m with a smaller ice crystal (< 50 cm^{-3}) and cloud droplet (< 50 cm^{-3}) number concentration. This is in the region of the cloud base and the cloud volume is strongly diluted and filamented possibly due to turbulent mixing with clear air as it was also observed in Beals et al. (2015).

5 Discussion and further improvements

5.1 Observation of meteorological parameters

As described in section 2 the wind measurements of the 3D Sonic Anemometer have to be corrected for movement of the cable car. In Fig. 7 the corrected wind speed and direction is compared to the MeteoSwiss wind measurements at the Eggishorn. However, this comparison has to be done carefully because of the influence of the local orography on the wind measurements and greater distance between the measurements with decreasing altitude of the cable car. From Fig. 7 there seems to be a systematic discrepancy in the wind direction. The reason for this is probably the orography just below the top station. The cable car moves along a valley and may explain the deviation of the wind direction at this altitude. At lower altitudes, when the cable car is moving more freely above the surface the corrected wind direction is in better agreement with the MeteoSwiss measurements.

Temperature data is available from the heated and ventilated temperature sensor (Rotronic) as well as the 3D Sonic Anemometer. The temperature profile of the temperature sensor shows a delayed response to the temperature change during a cable car ride. For this reason the reported ambient temperature in Fig. 7 is calculated from the virtual temperature T_v measured with the 3D Sonic Anemometer using

$$T = T_\mathrm{v} \frac{0.622\,(1+w)}{w+0.622} \quad , \tag{6}$$

with the water vapor mixing ratio w in $\mathrm{kg\,kg}^{-1}$ air. The corrected temperature in the highest altitude level is in accordance with the MeteoSwiss data (Fig. 7). In addition the difference in temperature between the altitude levels of 2850 m and 2250 m is 3.5 K according to the corrected temperature data of the 3D Sonic Anemometer. An iterative calculation of the temperature difference based on the saturated adiabatic lapse yields 4.2 K. Given that the measured temperature difference is less than the saturated adiabatic lapse rate suggests that the air was absolutely stable somewhere along the ride.

5.2 Observation of microphysical parameters

Laboratory measurements with the HOLIMO 3G instrument have shown its capability to resolve spherical particles larger than 6.2 µm (Fig. 4). Manual inspection by eye of the cloud particles classified as cloud droplets by the HOLOSuite software has shown that the HOLIMO 3G in combination with the HOLOSuite software is capable to reliably observe cloud droplets starting at a size of 6.5 µm. This is ~~particular~~ remarkable for the run at 13:51 on 23 February 2016 when the CDNC is as high

as 400 cm^{-3}. In such conditions a total of 2500 cloud droplets are present in the volume in-between the towers of HOLIMO 3G and therefore in a single hologram and increase the noise level significantly. Nevertheless, cloud droplets as small as 6.5 $\mu\mathrm{m}$ are reliably observed in this case. Although liquid droplets of a size on the order of millimeters were not present in the example data presented, the HOLIMO 3G is capable to detect particles in the size range of several micrometers to millimeters.

Phase separation is only possible for cloud particles larger than 35 $\mu\mathrm{m}$ for the field campaign in 2015. This is a result of mechanical instabilities of the optical set-up of the HOLIMO 3G instrument, which caused an increased background in the holograms and phase separation was significantly more difficult. After the field campaign in 2015 the optical set-up has been improved to a more rigid design, which reduces the background in the holograms. As a result a phase separation is possible for cloud particles starting at a size of 25 $\mu\mathrm{m}$ for the field campaign in 2016.

The spatial distribution of the cloud droplets and ice crystals of two example holograms is shown in Fig. 11. As described in the work of Beals et al. (2015), the investigation of local inhomogeneities in the spatial distribution of cloud droplets and ice crystals on a centimeter scale as well as the droplet size distribution of single holograms is possible with this unique feature of holography. A better understanding of the influence of turbulent mixing of a cloud with its environment on the spatial distribution of the cloud particles is of importance, because it influences for example the precipitation efficiency of a cloud. Upcoming analysis of the HoloGondel data will also focus on this topic especially when the cable car is leaving or entering a cloud during a run.

The vertical resolution of the HoloGondel platform depends on the vertical velocity of the cable car. With ~~an~~ a vertical distance of 650 m covered within in 200 s the cable car at the Eggishorn has a mean vertical velocity of 3.25 $\mathrm{m\,s}^{-1}$. Because ten holograms are grouped together for counting statistic reasons and with a frame rate of 6 fps, this results in a maximal vertical resolution of 5 m as presented in Fig. 9 for the vertical profile of the run at 13:31 on 23 February 2016. In addition to the variability of the spatial distribution on the centimeter scale the variation of the microphysical properties on a meter scale is possible. A sudden increase in the ICNC on this length scale for example can be an evidence for a secondary ice multiplication process.

The temporal resolution of the HoloGondel platform is limited by the interval between to runs of the cable car, which is on the order of 10 - 15 minutes and the wind speed. In the case of the Eggishorn the cable car runs every 20 minutes (Fig. 7 and 10) and with a wind speed on the order of a few ms^{-1} this results in a resolution of several kilometers.

In combination with the vertical profiles of the meteorological parameters the dependency ~~of~~ the microphysical properties of a cloud for example on the temperature, wind speed or turbulence can be analyzed. Especially the relationship between the temperature and the observed ICNC is of an interest for possible ice multiplication mechanisms. Because the height above the surface of the cable car is not constant during a run of the cable car the dependency of the microphysical parameters on the distance above the surface will be an additional point of interest. Lloyd et al. (2015) suggested an surface based process to explain the high ICNC observed at the Jungfraujoch. The dependency of the ICNC on the height above the surface of the HoloGondel platform may contribute to a better understanding of such processes and the importance of the influence at larger distances above the surface. Finally the measurements on a cable car can easily be repeated over a time interval of several years.

5.3 General issues of ~~in-sit~~ cloud observations on a cable car

The first two field campaigns at the Eggishorn also revealed some unexpected difficulties when it comes to in-situ cloud observation on a cable car cabin. First, the battery of the HoloGondel platform has to be recharged at least every second night. To be able to recharge the battery the cable car cabin with the HoloGondel platform on top has to be in the lower station and it is desirable that the operator of the cable car recharges the batteries because this way the user of the HoloGondel platform does not have to be present during the entire field campaign. During the three months time period of the field campaign in 2016 the HoloGondel platform only ran out of power twice. This was the case when the employees of the ski resort had to prepare the slopes over night and the cable car cabin with the HoloGondel platform was parked in the top station. Second, cable cars in ski resort operate on a more irregular schedule during cloudy conditions because of the absence of tourists. In the case of the Eggishorn the cable car was operated less than 50 % of the regular schedule. However, since the HoloGondel platform is able to operate unattended for weeks - it is remotely accessible, the data is automatically transferred to the local serve and the battery can easily be recharged by the cable car staff - a vast data set of vertical profiles is still achievable. In addition, there is usually the option to pay for extra runs of the cable car for a reasonable price on the order 50 SFR. An alternative to a large cable car in a ski resort could be a small supply cable car, which can be operated on demand. Summarizing the experience of the field campaigns with the HoloGondel platform at the Eggishorn, the success of a field campaign also depends on the employees of cable car company. In the case of the field campaigns at the Eggishorn in the winters 2015 and 2016 the support by the employees of the Luftseilbahnen Fiesch-Eggishorn AG was excellent.

6 Conclusions

The novel HoloGondel platform is described and example measurements of a liquid and a mixed-phase cloud at the Eggishorn in the Swiss Alps are discussed. The main findings are:

- HoloGondel is the first measurement platform to successfully observe vertical profiles of microphysical and meteorological cloud properties and their temporal evolution on a cable car during two field campaigns at the Eggishorn in the Swiss Alps.
- The findings of the Liquid Case on 23 February 2016 show that cloud droplets larger than 6.5 µm in a cloud with a number concentration as high as 400 cm^{-1} can reliably be observed with HOLIMO 3G, the main component of the HoloGondel platform.
- For the Mixed-Phase Case on 21 March 2015 separation between liquid droplets and ice crystals is possible for particles larger than 35 µm. An improvement of the design of HOLIMO 3G allows the separation for particles larger than 25 µm for the campaign in 2016.

- HOLIMO 3G is ~~capable~~ to observe the spatial distribution of the cloud particles in the sample volume on a centimetre scale as shown in Fig.11. The observation of the inhomogeneities of the spatial distribution of the cloud particles allows the investigation of the influence of entrainment and turbulent mixing on the development of a cloud.

- The HoloGondel platform is ~~capable~~ to observe the inhomogeneities and variability of the microphysical cloud parameters from a centimeter scale up to several kilometers. The spatial distribution of the cloud particles in the sample volume can be observed on a centimeter scale, whereas the vertical resolution is on the order of several meters. The temporal evolution is determined by the cable car schedule an is on the order of 10 - 15 minutes and corresponds to a resolution of several kilometers in the horizontal extend of the cloud.

- The high availability of measurements with the HoloGondel platform due to its low maintenance requirements ensures to observe a vast set of vertical profiles. In addition, the measurements can easily repeated at the same place over several years.

- With its modular design the measurements with the HoloGondel platform can easily be adjusted to the needs of its users only limited by weight and power restrictions. The observations of vertical profiles can for example be extended to aerosol measurements or additional cloud probes.

The HoloGondel platform as ~~an~~ unique approach to observe the vertical profiles of microphysical and meteorological properties of mixed-phase clouds in complex alpine terrain has shown its feasibility during the campaigns in 2015 and 2016 at the Eggishorn in the Swiss Alps. It overcomes the limitation of a single-point observation at mountain-top research stations and is ~~capable~~ to observe the cloud structure and inhomogeneities from a centimeter scale up to several kilometers. With the high availability and repeatability of the measurements the HoloGondel platform offers the opportunity to improve the understanding of microphysical processes in clouds (e.g. precipitation initiation and ice multiplication).

Acknowledgements. The authors are grateful to Jacob Fugal for many stimulating discussion about the design of the HoloGondel platform and his help in improving the manuscript. We would also like to thank Janina Stäudle for her assistance during the field campaign in winter 2015 and the following data analysis phase. The authors thank the Eggishorn-Fiescheralp Seilbahn AG staff for their excellent support during the field measurements. The meteorological measurements at the Eggishorn were provided by the Swiss Federal Office of Meteorology and Climatology MeteoSwiss. This project was supported by ETH Zurich under grant ETH-30 13-2.

References

Amsler, P., Stetzer, O., Schnaiter, M., Hesse, E., Benz, S., Moehler, O., and Lohmann, U.: Ice crystal habits from cloud chamber studies obtained by in-line holographic microscopy related to depolarization measurements, Appl. Optics, 48, 5811–5822, doi:10.1364/AO.48.005811, 2009.

Baumann, K., Maurer, H., Rau, G., Piringer, M., Pechinger, U., Prévôt, A., Furger, M., Neininger, B., and Pellegrini, U.: The influence of south Foehn on the ozone distribution in the Alpine Rhine valley—results from the {MAP} field phase, Atmos. Environ., 35, 6379 – 6390, doi:10.1016/S1352-2310(01)00364-8, 2001.

Baumgardner, D., Brenguier, J., Bucholtz, A., Coe, H., DeMott, P., Garrett, T., Gayet, J., Hermann, M., Heymsfield, A., Korolev, A., Krämer, M., Petzold, A., Strapp, W., Pilewskie, P., Taylor, J., Twohy, C., Wendisch, M., Bachalo, W., and Chuang, P.: Airborne instruments to measure atmospheric aerosol particles, clouds and radiation: A cook's tour of mature and emerging technology, Atmos. Res., 102, 10 – 29, doi:10.1016/j.atmosres.2011.06.021, 2011.

Baumgardner, D., Avallone, L., Bansemer, A., Borrmann, S., Brown, P., Bundke, U., Chuang, P. Y., Cziczo, D., Field, P., Gallagher, M., Gayet, J.-F., Heymsfield, A., Korolev, A., Krämer, M., McFarquhar, G., Mertes, S., Möhler, O., Lance, S., Lawson, P., Petters, M. D., Pratt, K., Roberts, G., Rogers, D., Stetzer, O., Stith, J., Strapp, W., Twohy, C., and Wendisch, M.: In Situ, Airborne Instrumentation: Addressing and Solving Measurement Problems in Ice Clouds, B. Am. Meteorol. Soc., 93, ES29–ES34, doi:10.1175/BAMS-D-11-00123.1, 2012.

Beals, M. J., Fugal, J. P., Shaw, R. a., Lu, J., Spuler, S. M., and Stith, J. L.: Holographic measurements of inhomogeneous cloud mixing at the centimeter scale, Science, 350, 87–90, doi:10.1126/science.aab0751, 2015.

Bergeron, T.: On the physics of clouds and precipitation, in: Proces Verbaux de l'Association de Météorologie, Int. Union of Geodesy and Geophys., 156–178, 1935.

Conway, B., Caughey, S., Bentley, A., and Turton, J.: Ground-based and airborne holography of ice and water clouds, Atmos. Environ., 16, 1193 – 1207, doi:10.1016/0004-6981(82)90208-6, 1982.

Farrington, R. J., Connolly, P. J., Lloyd, G., Bower, K. N., Flynn, M. J., Gallagher, M. W., Field, P. R., Dearden, C., and Choularton, T. W.: Comparing model and measured ice crystal concentrations in orographic clouds during the INUPIAQ campaign, Atmospheric Chemistry and Physics Discussions, 15, 25 647–25 694, doi:10.5194/acpd-15-25647-2015, 2015.

Findeisen, W.: Kolloid-meteorologische Vorgänge bei Neiderschlagsbildung, Meteor. Z, 55, 121–133, 1938.

Flato, G., Marotzke, J., Abiodun, B., Braconnot, P., Chou, S., Collins, W., Cox, P., Driouech, F., Emori, S., Eyring, V., Forest, C., Gleckler, P., Guilyardi, E., Jakob, C., Kattsov, V., Reason, C., and Rummukainen, M.: Evaluation of Climate Models, in: Climate Change 2013: The Physical Science Basis. Contribution of Working Group I to the Fifth Assessment Report of the Intergovernmental Panel on Climate Change, pp. 741–866, Cambridge University Press, Cambridge, United Kingdom and New York, NY, USA, doi:10.1017/CBO9781107415324.020, 2013.

Fugal, J. P.: HOLOSuite, in preparation, 2016.

Fugal, J. P. and Shaw, R. A.: Cloud particle size distributions measured with an airborne digital in-line holographic instrument, Atmos. Meas. Tech., 2, 259–271, doi:10.5194/amt-2-259-2009, 2009b.

Fugal, J. P., Schulz, T. J., and Shaw, R. A.: Practical methods for automated reconstruction and characterization of particles in digital in-line holograms, Measurement Science and Technology, 20, 075 501, 2009a.

Geerts, B., Pokharel, B., and Kristovich, D. a. R.: Blowing Snow as a Natural Glaciogenic Cloud Seeding Mechanism, Mon. Weather Rev., 143, 5017–5033, doi:10.1175/MWR-D-15-0241.1, 2015.

Gultepe, I. and Zhou, B.: FTS (Fog To Snow) Conversion Process During the SNOW-V10 Project, Pure Appl. Geophys., 169, 783–791, doi:10.1007/s00024-011-0349-4, 2011.

Hallet, J. and Mossop, S.: Production of secondary ice particles during the riming process, Nature, 249, 26–28, doi:10.1038/249026a0, 1974.

Henneberger, J.: Mountain-top in-situ observations of mixed-phase clouds with a digital holographic instrument, Ph.D. thesis, ETH Zurich, Switzerland, 2013a.

Henneberger, J., Fugal, J. P., Stetzer, O., and Lohmann, U.: HOLIMO II: a digital holographic instrument for ground-based in situ observations of microphysical properties of mixed-phase clouds, Atmos. Meas. Tech., 6, doi:10.5194/amt-6-2975-2013, 2013b.

Heymsfield, A. and Willis, P.: Cloud Conditions Favoring Secondary Ice Particle Production in Tropical Maritime Convection, J. Atmos. Sci., 71, 4500–4526, doi:10.1175/JAS-D-14-0093.1, 2014.

Joe, P., Scott, B., Doyle, C., Isaac, G., Gultepe, I., Forsyth, D., Cober, S., Campos, E., Heckman, I., Donaldson, N., Hudak, D., Rasmussen, R., Kucera, P., Stewart, R., Thériault, J. M., Fisico, T., Rasmussen, K. L., Carmichael, H., Laplante, A., Bailey, M., and Boudala, F.: The Monitoring Network of the Vancouver 2010 Olympics, Pure Appl. Geophys., 171, 25–58, doi:10.1007/s00024-012-0588-z, 2012.

Lawson, R. P., Stamnes, K., Stamnes, J., Zmarzly, P., Koskuliks, J., Roden, C., Mo, Q., Carrithers, M., and Bland, G. L.: Deployment of a Tethered-Balloon System for Microphysics and Radiative Measurements in Mixed-Phase Clouds at Ny-Ålesund and South Pole, J. Atmos. Ocean. Tech., 28, 656–670, doi:10.1175/2010JTECHA1439.1, 2011.

Lawson, R. P., Woods, S., and Morrison, H.: The Microphysics of Ice and Precipitation Development in Tropical Cumulus Clouds, Journal of the Atmospheric Sciences, 72, 2429–2445, doi:10.1175/JAS-D-14-0274.1, 2015.

Lloyd, G., Choularton, T. W., Bower, K. N., Gallagher, M. W., Connolly, P. J., Flynn, M., Farrington, R., Crosier, J., Schlenczek, O., Fugal, J., and Henneberger, J.: The origins of ice crystals measured in mixed-phase clouds at the high-alpine site Jungfraujoch, Atmos. Chem. Phys., 15, 12 953–12 969, doi:10.5194/acp-15-12953-2015, 2015.

Lohmann, U., Felix, L., and Mahrt, F.: An Introduction to clouds: from the microscale to the climate, Camebridge University Press, Cambridge, United Kingdom, 2016.

Lu, J., Fugal, J. P., Nordsiek, H., Saw, E. W., Shaw, R. A., and Yang, W.: Lagrangian particle tracking in three dimensions via single-camera in-line digital holography, New J. Phys., 10, 125 013, 2008.

McFarlane, S. A. and Grabowski, W. W.: Optical properties of shallow tropical cumuli derived from ARM ground-based remote sensing, Geophy. Res. Lett., 34, n/a–n/a, doi:10.1029/2006GL028767, 2007.

Morrison, H., de Boer, G., Feingold, G., Harrington, J., Shupe, M. D., and Sulia, K.: Resilience of persistent Arctic mixed-phase clouds, Nature Geoscience, 5, 11–17, doi:doi:10.1038/ngeo1332, 2012.

Piringer, M., Baumann, K., Pechinger, U., and Vogt, S.: Meteorological and ozone sounding experience during a strong foehn event a MAP case study, Meteorol. Z., 10, 445–455, doi:10.1127/0941-2948/2001/0010-0445, 2001.

Raupach, S. M. F., Vössing, H. J., Curtius, J., and Borrmann, S.: Digital crossed-beam holography for in situ imaging of atmospheric ice particles, J. Opt. A-Pure Appl. Op., 8, 796, 2006.

Reiter, R.: Upward flux of RaB and RaC in the planetary boundary layer as controlled by atmospheric microstructure, Pure Appl. Geophy., 72, 247–258, doi:10.1007/BF00875708, 1967.

Reiter, R. and Carnuth, W.: Comparing lidar reflectivity profiles against measured profiles of vertical aerosol distribution between 1 and 3 km a. s. l., Arch. Meteor. Geophy. A, 24, 69–92, doi:10.1007/BF02247559, 1975.

Rogers, D. C. and Vali, G.: Ice Crystal Production by Mountain Surfaces, J. Clim. Appl. Meteorol., 26, 1152–1168, doi:10.1175/1520-0450(1987)026<1152:ICPBMS>2.0.CO;2, 1987.

Schumann, U., Fahey, D. W., Wendisch, M., and Brenguier, J.-L.: Introduction to Airborne Measurements of the Earth Atmosphere and Surface, pp. 1–5, Wiley-VCH Verlag GmbH & Co. KGaA, doi:10.1002/9783527653218.ch1, 2013.

Shupe, M. D., Daniel, J. S., de Boer, G., Eloranta, E. W., Kollias, P., Luke, E. P., Long, C. N., Turner, D. D., and Verlinde, J.: A Focus On Mixed-Phase Clouds, B. Am. Meteorol. Soc., 89, 1549–1562, doi:10.1175/2008BAMS2378.1, 2008.

Siebert, H., Lehmann, K., Wendisch, M., Franke, H., Maser, R., Schell, D., Saw, E. W., and Shaw, R. A.: Probing Finescale Dynamics and Microphysics of Clouds with Helicopter-Borne Measurements, B. Am. Meteorol. Soc., 87, 1727–1738, doi:10.1175/BAMS-87-12-1727, 2006.

Sikand, M., Koskulics, J., Stamnes, K., Hamre, B., Stamnes, J. J., and Lawson, R. P.: Estimation of Mixed-Phase Cloud Optical Depth and Position Using In Situ Radiation and Cloud Microphysical Measurements Obtained from a Tethered-Balloon Platform, J. Atmos. Sci., 70, 317–329, doi:10.1175/JAS-D-12-063.1, 2013.

Spuler, S. M. and Fugal, J.: Design of an in-line, digital holographic imaging system for airborne measurement of clouds, Appl. Opt., 50, 1405–1412, doi:10.1364/AO.50.001405, 2011.

Sun, Z. and Shine, K. P.: Studies of the radiative properties of ice and mixed-phase clouds, Q. J. Roy. Meteor. Soc., 120, 111–137, doi:10.1002/qj.49712051508, 1994.

Uchiyama, A., Yamazaki, A., Shiobara, M., and Kobayashi, H.: Case study on microphysical properties of boundary layer mixed-phase cloud observed at Ny-Ålesund, Svalbard: Observed cloud microphysics and calculated optical properties on 9 June 2011, Polar Science, 8, 57 – 72, doi:http://dx.doi.org/10.1016/j.polar.2013.11.001, 2014.

Verlinde, J., Harrington, J. Y., Yannuzzi, V. T., Avramov, A., Greenberg, S., Richardson, S. J., Bahrmann, C. P., McFarquhar, G. M., Zhang, G., Johnson, N., Poellot, M. R., Mather, J. H., Turner, D. D., Eloranta, E. W., Tobin, D. C., Holz, R., Zak, B. D., Ivey, M. D., Prenni, A. J., DeMott, P. J., Daniel, J. S., Kok, G. L., Sassen, K., Spangenberg, D., Minnis, P., Tooman, T. P., Shupe, M., Heymsfield, A. J., and Schofield, R.: The Mixed-Phase Arctic Cloud Experiment, B. Am. Meteorol. Soc., 88, 205–221, doi:10.1175/BAMS-88-2-205, 2007.

Vidaurre, G. and Hallett, J.: Ice and water content of stratiform mixed-phase cloud, Q. J. Roy. Meteor. Soc., 135, 1292–1306, doi:10.1002/qj.440, 2009.

Vochezer, P., Järvinen, E., Wagner, R., Kupiszewski, P., Leisner, T., and Schnaiter, M.: In situ characterization of mixed phase clouds using the Small Ice Detector and the Particle Phase Discriminator, Atmos. Meas. Tech., 9, 159–177, doi:10.5194/amt-9-159-2016, 2016.

Wegener, A.: Thermodynamik der Atmosphäre, Barth, Leipzig, 1911.

Zhang, D., Wang, Z., and Liu, D.: A global view of midlevel liquid-layer topped stratiform cloud distribution and phase partition from CALIPSO and CloudSat measurements, J. Geophys. Res-Atmos., 115, n/a–n/a, doi:10.1029/2009JD012143, 2010.

Table 1. Summary of the instruments mounted on the HoloGondel platform and their observables.

Instrument	Observable
HOLIMO 3G	Size distribution
	Particle concentration
	Water content
	Spatial distribution
	Ice crystal shape
3D Sonic Anemometer, Theiss	Wind velocity and direction
	Turbulence
	Virtual Temperature
HygroMet4, Rotronic	Temperature
	Relative humidity
GPS, GlobalSat	Location
	Velocity above ground

Table 2. Comparison of the results of the calibration measurements of HOLIMO 3G with the results of an Aerodynamic Particle Sizer (APS, TSI, Minnesota USA) and the data provided by the manufacturer from a COULTER Multisizer 3. The uncertainties of the HOLIMO 3G and APS data was calculated from a Gaussian fit to the normalized size distribution.

	particle diameter (μm)		
Multisizer	6.40 ± 0.11	10.25 ± 0.19	18.23 ± 0.24
HOLIMO 3G	7.32 ± 1.95	10.48 ± 1.34	18.10 ± 1.67
APS	6.56 ± 0.29	10.12 ± 0.67	17.93 ± 1.35

Table 3. Overview of the technical parameters of the cable car Fiescheralp - Eggishorn.

Altitude bottom station (Fiescheralp)	2217 m.a.s.l.
Altitude top station (Eggishorn)	2871 m.a.s.l.
Vertical distance	654 m
Horizontal distance	1716 m
Average slope	38 %
Maximal slope	57 %
Average speed	$10\,\mathrm{m\,s^{-1}}$
Average travel time	200 s

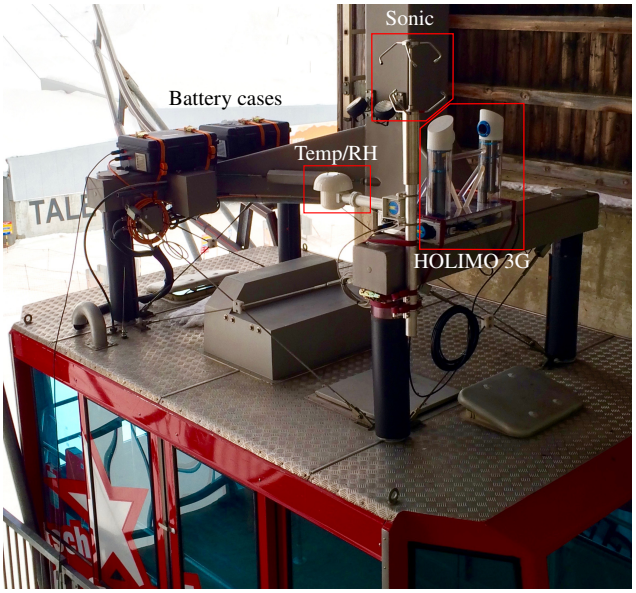

Figure 1. Experimental set up of the HoloGondel platform during the measurement campaign at the Eggishorn in the winter season 2016/2017. The picture was taken in the lower station of the cable car in Fiescheralp. The GPS Sensor is not visible on this picture, because it is mounted on the opposite side of the crossbar.

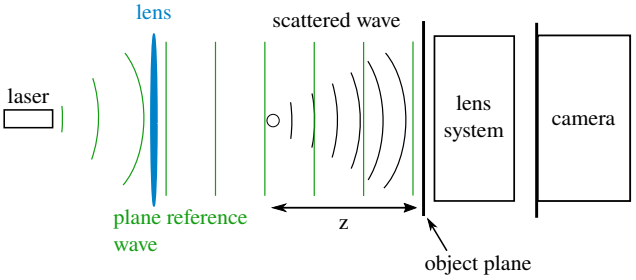

Figure 2. Schematic of the working principle of digital in-line holography: The reference wave emitted by a laser is collimated using a convex lens. The plane reference wave is scattered by a particle and interferes with the generated scattered wave to form an interference pattern. To improve the resolution of the system, the interference pattern in the object plane is magnified with a lens system and projected on the sensor of the camera.

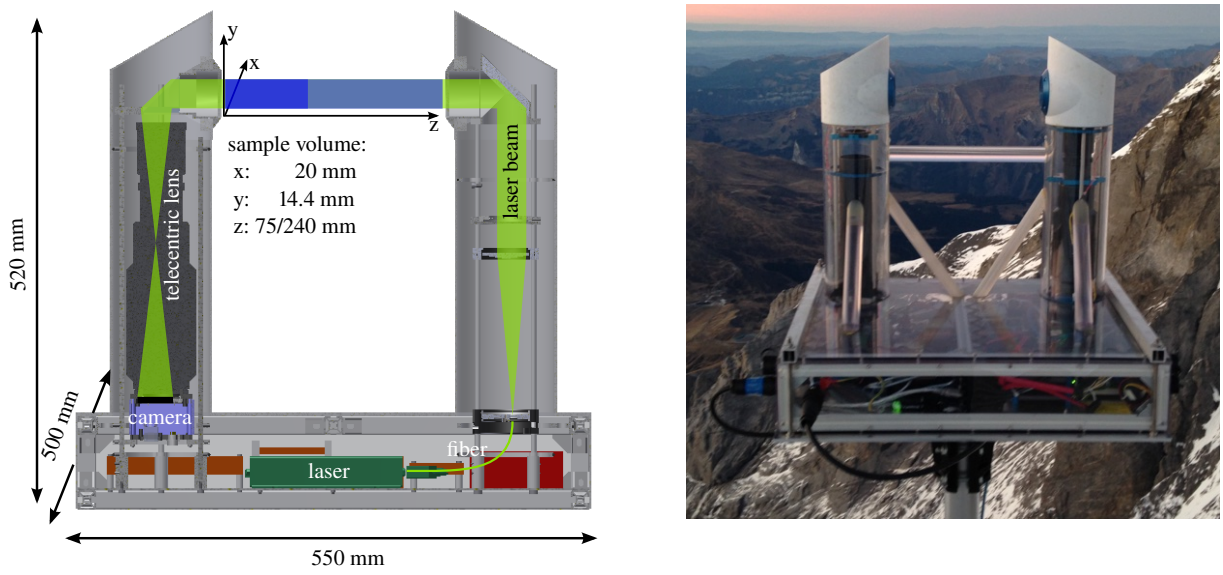

Figure 3. Technical drawing (left) and a picture (right) of the HOLIMO 3G instrument with its main components. The ambient air can stream freely between the two towers and the detection volume is the field of view of the instrument between the two towers. The dark blue box indicates the sample volume with the highest resolution of 6.2 µm and a depth of 75 mm. The dark and light blue box indicate the entire sample volume in-between the two towers with a depth of 240 mm and a resolution of 20 µm.

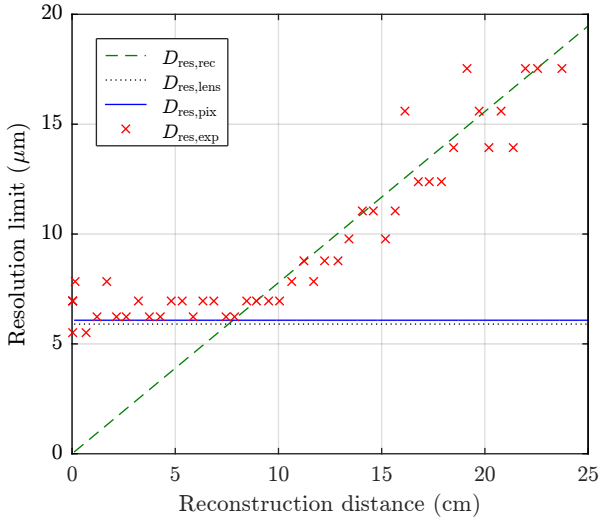

Figure 4. Resolution measurements of the HOLIMO 3G instrument versus reconstruction distance z. The three lines indicate theoretical calculations for the resolution limit due to the pixel size ($D_{res,rec}$), the optical limitation of the lens system ($D_{res,lens}$) and the optical setup of the instrument ($D_{res,rec}$).

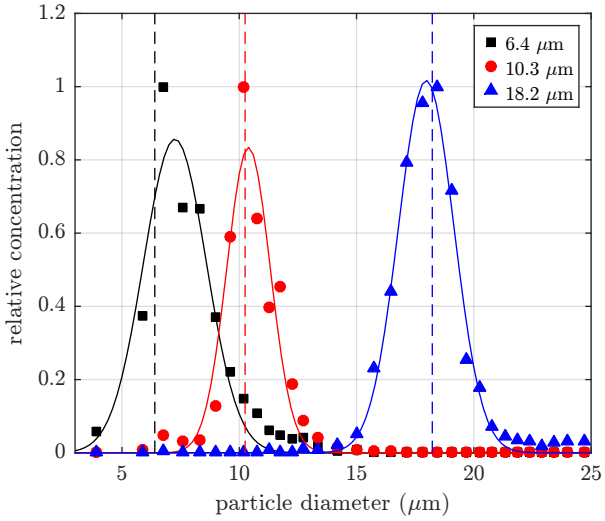

Figure 5. Result of the calibration measurement for HOLIMO 3G with monodisperse spheres with diameters of 6.4, 10.3 and 18.2 µm. The dots represent the normalized concentrations measured by HOLIMO 3G. A Gaussian distribution is fitted (solid line) and compared to the nominal size (dashed line).

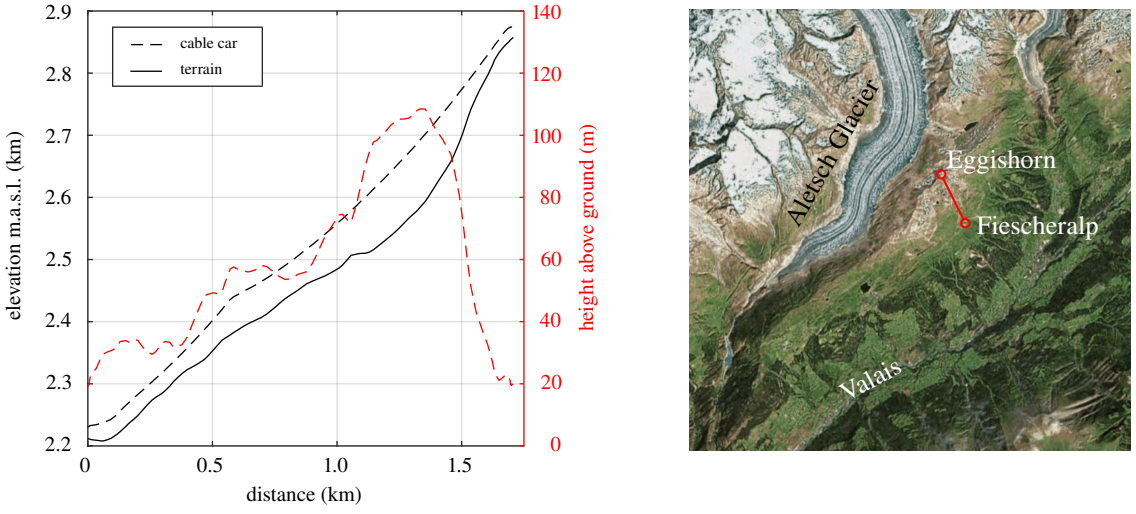

Figure 6. Left: Profile of the terrain (solid black line) and a ride of the cable car (dashed black line) together with the height of the cable car above the surface (solid red line). **Right:** Map of the measurement site.

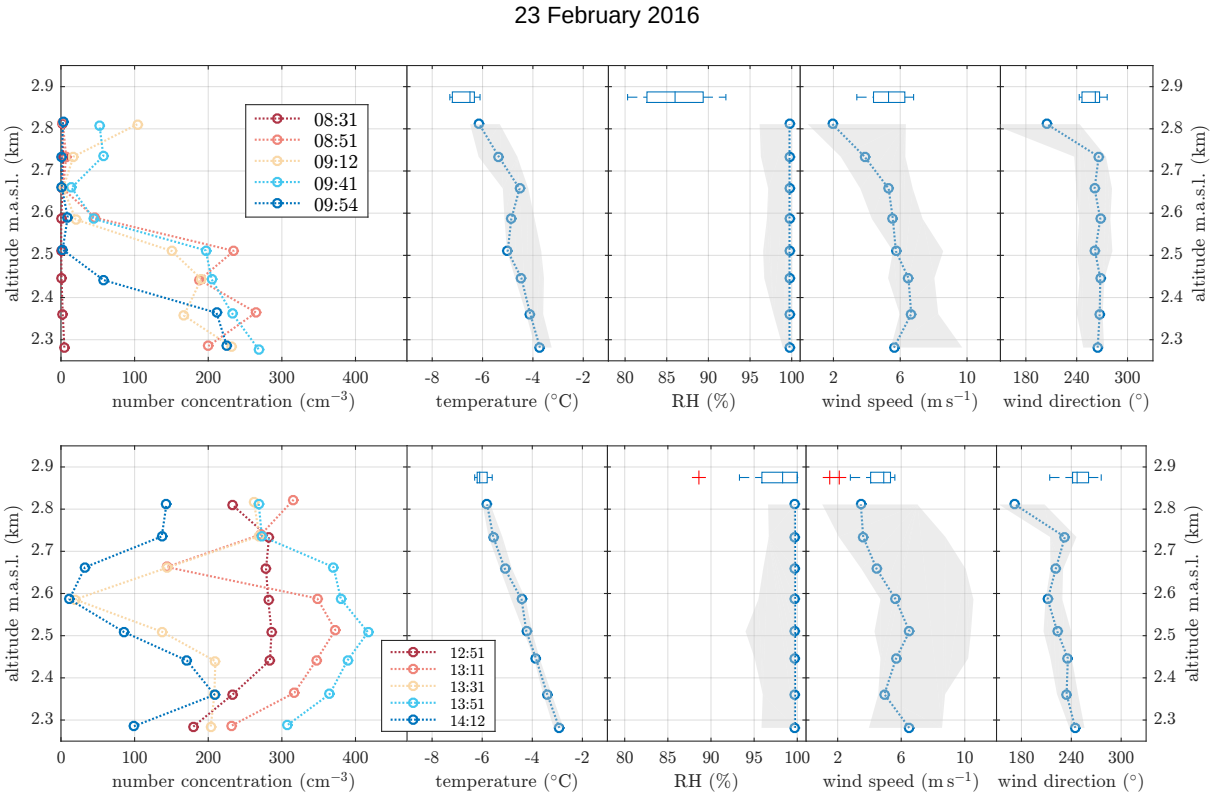

Figure 7. Height profiles of the Liquid Case measured with the HoloGondel platform during the morning (top) and the afternoon (bottom) of 23 February 2016. The data is averaged over an altitude interval of 75 m. The number concentration of cloud droplets (left panel) shows individual runs of the cable car. For the meteorological parameters (four right panels) the median (circle), the minimum and the maximum (shaded area) values of the vertical intervals are shown. The boxplots indicate the data of the MeteoSwiss station at the Eggishorn about 50 m above the cable car station for comparison. For each box, the central line marks the median value of the measurement and the left and right edges of the box represent 25th and the 75th percentiles respectively. The whiskers extend to minimum and maximum of the data, whereas outliers are marked as red pluses.

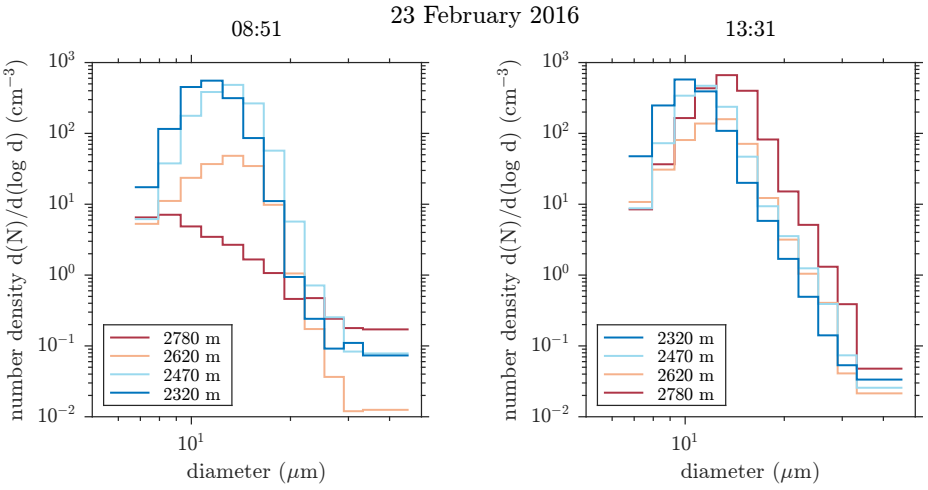

Figure 8. Height resolved cloud droplet size distribution during the 8:51 run in the morning (**left**) and the 13:31 run in the afternoon . The data was averaged over an altitude interval of 150 m.

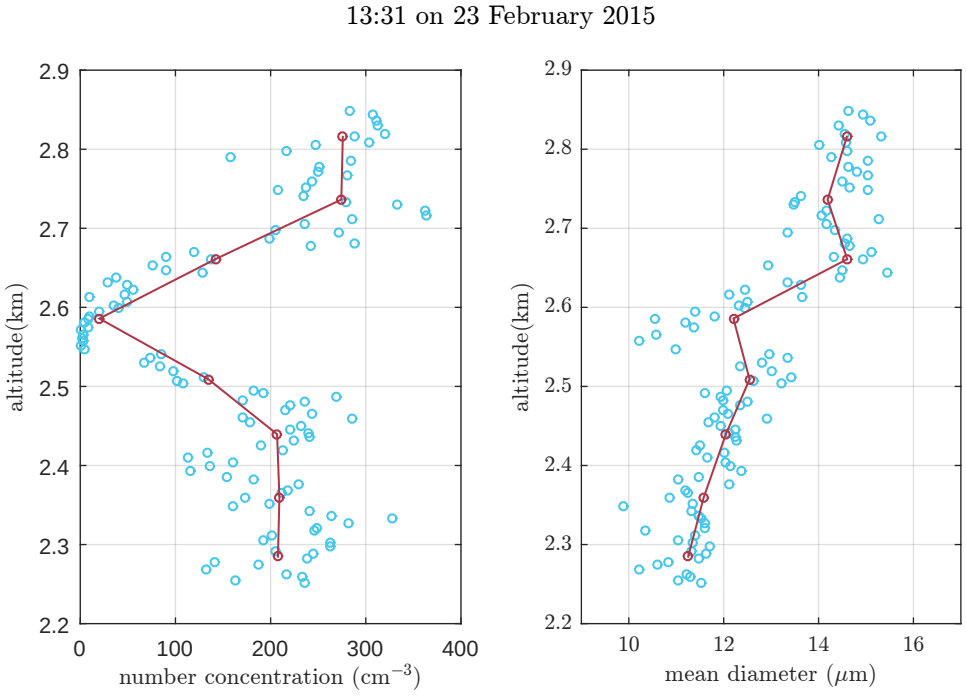

Figure 9. Comparison of two vertical profiles for the cloud droplet number concentration (**left**) and mean cloud droplet diameter (**right**) for the run at 13:31 on February 2015. The vertical profiles in blue show the maximal vertical resolution of the HoloGondel platform of 5 m. The vertical profiles in red are averaged over an vertical interval of 75 m.

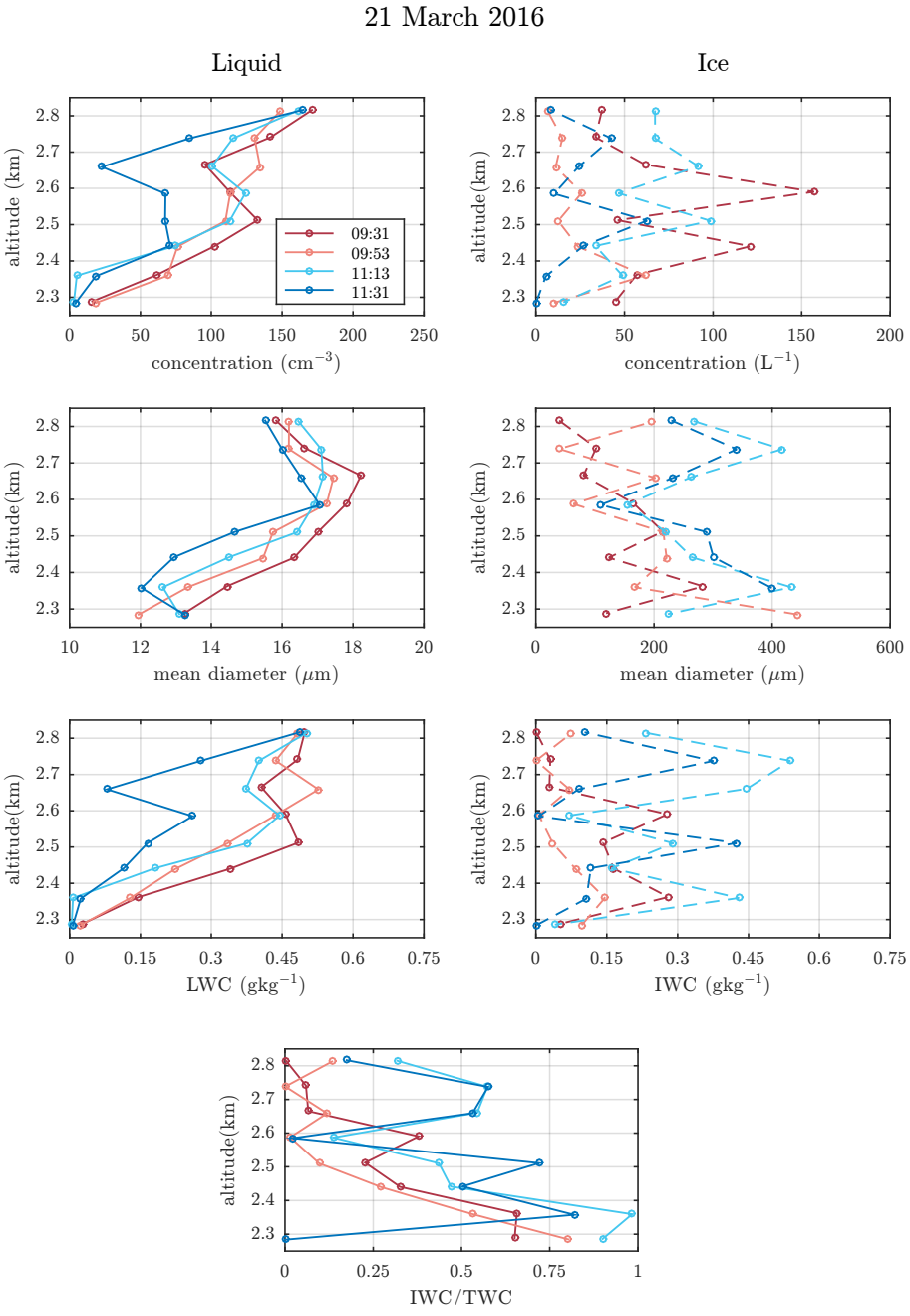

Figure 10. Height profiles of the cloud droplet (**left**) and ice crystal (**right**) number concentration, mean diameter and water content and the ratio of the ice water content to total water content (**bottom**) on 21 March 2015. The data is averaged over an altitude interval of 75 m.

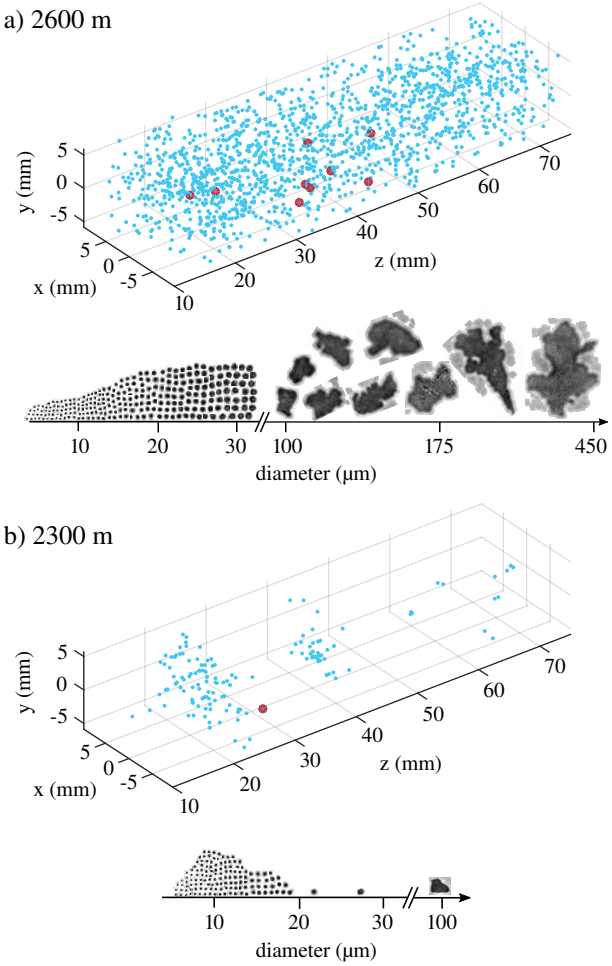

Figure 11. Spatial distribution of the liquid droplets (blue) and ice crystals (red) and examples of the two dimensional shadowgraphs for two holograms captured at an altitude of 2600 m **(a)** and 2300 m **(b)** at 9:31 on 21 March 2015. Whereas the liquid droplets are distributed uniformly in the sample volume at an altitude of 2600 m, the sample volume at 2300 m is strongly diluted and filamented.